OPTIMIZING SOLAR WATER HEATER PERFORMANCE THROUGH A NUMERICAL STUDY OF ZIG-ZAG SHAPED TUBES

by

Mohammed Choukri KORTI[a], Ahmed YOUCEF[a], Ali AKGUL[b,c*], Adil Abbas ALWAN[d], Karrar S. MOHSEN[e], Jihad ASAD[f], Rabab JARRAR[f], Hussein SHANAK[f], Younes MENNI[g], and Sherzod ABDULLAEV[h,i]

[a] Research Unit for Renewable Energies in the Saharan Region (URERMS), Renewable Energy Development Center (CDER), Adrar, Algeria
[b] Department of Mathematics, Art and Science Faculty, Siirt University, Siirt, Turkey
[c] Department of Electronics and Communication Engineering, Saveetha School of Engineering, SIMATS, Chennai, Tamilnadu, India
[d] Collage of Engineering, National University of Science and Technology, Dhi Qar, Iraq
[e] Information and Communication Technology Research Group, Scientific Research Center, Al-Ayen University, Thi-Qar, Iraq
[f] Department of Physics, Faculty of Applied Science, Palestine Technical University-Kadoorie, Tulkarm, Palestine
[g] Department of Technology, University Center Salhi Ahmed Naama (Ctr. Univ. Naama), Naama, Algeria
[h] Faculty of Chemical Engineering, New Uzbekistan University, Tashkent, Uzbekistan
[i] Department of Science and Innovation, Tashkent State Pedagogical University named after Nizami, Tashkent, Uzbekistan

Original scientific paper
https://doi.org/10.2298/TSCI2304143K

This study aimed to investigate the thermal behavior of water flows in a solar collector equipped with zig-zag tubes. To achieve this, a numerical simulation using CFD was conducted, which is a powerful tool for analyzing fluid-flow and heat transfer. The simulation employed the finite volume method to discretize the fluid domain and the SIMPLE algorithm to solve the pressure-velocity coupling. The simulation results indicated that the shape of the tubes significantly influenced the flow behavior and overall performance of the solar collector. Specifically, the temperature profiles at various times of the day showed that zig-zag-shaped tubes enhanced the heat transfer coefficient, resulting in higher temperatures within the collector. Moreover, the zig-zag design increased the residence time of the fluid inside the collector, further improving its overall efficiency. These findings highlight the potential of utilizing zig-zag-shaped tubes to optimize the performance of solar water heating systems, which could have important implications for renewable energy applications.

Key words: *solar energy, solar collector, zig-zag tubes, modelisation, simulation*

Introduction

A solar water heater is an innovative and sustainable device that harnesses solar energy to produce hot water using low to moderate temperatures. It works by converting sun-

* Corresponding author, e-mail: aliakgul00727@gmail.com

light into heat, which is then transferred to the water through a heat exchanger. This technology is becoming increasingly popular due to its high energy efficiency, low operating costs, and environmental friendliness. In addition to producing hot water, solar water heaters can also be used in preheating systems, such as solar distillation, which is a process of purifying water by evaporating and condensing it using solar energy. Solar water heaters are ideal for residential and commercial applications, as well as for use in remote areas without access to conventional power sources. They provide a sustainable and reliable solution for meeting the hot water demand while reducing greenhouse gas emissions and dependence on fossil fuels.

Li *et al.* [1] have shown that a combination of air source heat pump and solar evacuated tube water heater can be used as a winter heating system, presenting a novel approach to heating single rural buildings in cold regions. The research conducted by Tamuli *et al.* [2] demonstrates that incorporating phase change material in water heating leads to an increase in outlet temperature, resulting in a higher temperature at the end of the day. Nazari *et al.* [3] reveled that water heaters coated with CuO NS displayed superior performance when compared to water heaters featuring black or simple copper absorber plates. The research conducted by Siritan *et al.* [4] suggests that the most effective closed-loop pulsating heat pipe is characterized by an inner diameter of 1.50 mm, an evaporator length of 1.25 m, and 4 sets. Tamuli *et al.* [5] implemented innovative techniques to develop a solar water heater. Since the output of solar collectors is subject to changes in solar radiation, this variability must be considered in the analysis. In Sivasubramanian and colleagues' study [6], water was first analyzed using a solar water heater, yielding an outlet temperature of 355 K. Gudeta's objective [7] was to assess the effect of tilt angles on the collection of solar thermal energy in various cities, including comparisons of different tilt angles for the chosen locations.

Arun's study [8] aimed reduce heat loss and enhancing heat transfer in a solar collector tube. To achieve this, the geometry of the riser tube was modified by creating dimples along its surface, arranged in a circular pattern. Al-Joboory [9] demonstrated enhancements in overall daily efficiency of water heaters. Shalaby *et al.* [10] developed a novel heat storage system with other different situations. In a study by Deeyoko *et al.* [11], the performance of absorption tubes was investigated along side a thermal performance booster for a flat plate solar water heater. Balaji *et al.* [12] employed two types of thermal boosters, namely rod and tube, which were rubbed against a solar absorber tube. Tang *et al.* [13] showed that the reverse flow in a solar water heater was notably higher than that observed in a thermosyphonic domestic solar water heater fitted with flat-plate collectors. Wannagosit *et al.* [14] carried out a study on an evacuated tube solar water heater system that employed thermosyphon heat exchange, using both experimental and theoretical investigations. Li *et al.* [15] conducted a comprehensive assessment of the flow and heat transfer efficiency of solar water heaters by employing numerical simulation techniques. In a related study, Arab *et al.* [16] demonstrated the substantial potential for enhancing the performance of solar water heaters. They highlighted the remarkable economic benefits that can be achieved, with potential cost savings of up to 28%. Furthermore, Menni *et al.* [17, 18] conducted several numerical studies investigating different heat exchanger channels under various geometric conditions. A multitude of research endeavors have been carried out to improve the flow characteristics of air in diverse industrial settings, encompassing the domain of diesel engines. These examinations have aimed to maximize the efficiency of combustion, diminish emissions, and enhance the overall performance of the engine [19].

The geometric shape of the heat transfer fluid passage significantly affects the efficiency of solar collectors that use direct water-absorbent plate contact. This study focuses on

investigating the heat transfer between the absorbent wall and the heat transfer fluid in Z-shaped tubes arranged in parallel, aiming to improve the efficiency of the solar collector. The study uses different temperatures obtained during the day to analyze the heat transfer characteristics between the absorbent wall and the heat transfer fluid. By studying the heat transfer mechanism, the solar collector design can be optimized to improve its energy efficiency and cost-effectiveness. The study's findings can contribute to the development of solar thermal energy systems and advance sustainable and renewable energy technologies.

Comprehensive description of the model

Figure 1 depicts a schematic representation of a Z-shaped tube solar water heater, consisting of a box with length, *L*, width, *W*, and height, *H*. The solar collector includes seven copper tubes arranged in parallel beneath a copper absorber and a single white glass cover.

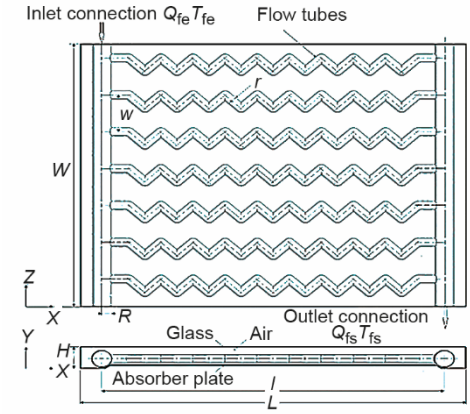

Figure 1. Graphical illustration of the present solar water heating system

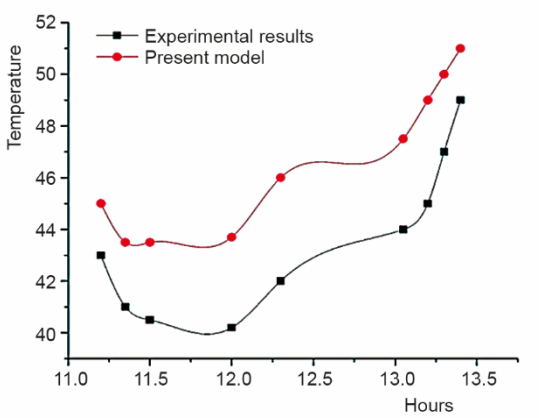

Figure 2. A comparison of the present CFD results with the experimental predictions made by [20]

The diagram presented in fig. 1 depicts a solar water heater with a Z-shaped tube design, which is an efficient and popular method for harnessing solar energy to heat water. This schematic representation visually outlines the structure of the system, including the key components and their interconnections, providing a clear understanding of how it functions.

The thermal insulation surrounding the collector is also illustrated, while the geometrical and physical parameters of the collector are listed in tabs. 1 and 2, respectively. The Z-shaped tube design aims to enhance the heat transfer between the absorber and the heat transfer fluid, thereby improving the overall efficiency of the solar water heater. This illustration provides a clear visualization of the key components of the solar water heater and their respective dimensions, which are crucial for accurate modeling and performance analysis.

Modeling and simulation

The mathematical framework for modeling fluid-flow and heat transfer is established through the following governing equations:

Continuity:

$$\frac{\partial(\rho u_i)}{\partial x_i} = 0 \tag{1}$$

Momentum:

$$\rho u_j \frac{\partial u_i}{\partial x_j} = -\frac{\partial P}{\partial x_i} + \frac{\partial}{\partial x_j}\left(\frac{\partial u_i}{\partial x_j} - \frac{\partial u_j}{\partial x_i}\right) \tag{2}$$

Energy:

$$c_p \frac{\partial(\rho u_i T)}{\partial x_j} = \lambda \frac{\partial}{\partial x_j}\left(\frac{\partial T}{\partial x_j}\right) \tag{3}$$

Table 1. The collector geometric parameters

Components	Size	Value
Box	H [cm]	4.5
	L [cm]	67.91
	W [cm]	61.43
Tubes	l [cm]	60.41
	r [cm]	1
	w [cm]	7.82
	n	7
Tube (intel, outlet)	L [cm]	61.43
	R [cm]	1.75
Isolation	$L \times W$ [cm^2]	$L \times W$

Table 2. Physical properties of the materials

Physical properties	Copper (absorber + pipes)	Rockwool (isolation)	Single white glass
ρ [kgm^{-3}]	8978	48	2500
Cp [Jkg^{-1} per °C]	381	840	720
λ [wm^{-1} per °C]	387.6	0.04	1
Absorption coefficient	0.9	0.9	0.1
Emissivity coefficient	0.2	0.2	0.93
Transmission coefficient	/	/	0.84

The CFD was employed as a powerful simulation tool to analyze fluid-flow and heat transfer in the system. The finite volume method was used to discretize the fluid domain, and the pressure-velocity coupling was solved using the SIMPLE algorithm. Before conducting the numerical analysis, the grid-independency of the system was assessed by varying the number of grids used. Eventually, the system was discretized into 1612054 elements to ensure both grid-independency and accuracy of the calculations. The outlet water temperature profiles at different times of the day obtained through the proposed numerical model were compared with those predicted experimentally by Patel *et al.* [20], as shown in fig. 2. The comparison reveals

a strong correlation between the results, demonstrating the accuracy of the proposed method. The average relative error between the values is 6.8%, indicating good agreement.

Findings and analysis

On January 5, 2021, the meteorological data of the Adrar region was measured experimentally by the URER/MS. If the yield obtained on this day of the year is deemed acceptable as a minimum, we can anticipate achieving even higher yields during other periods when the temperature reaches up to 50 °C. This highlights the potential for increased productivity and underscores the importance of further investigating the relationship between meteorological conditions and yield in the Adrar region.

At 08:00 a. m., fig. 3 illustrates the evolution of water temperature profiles at the center of the sensor on the (X, Z) plane, with ambient temperature T_{amb} = 274.75 K, direct normal irradiation D_i = 189 W/m², and diffuse horizontal irradiation D_H = 7 W/m². The figure shows a gradual increase in water temperature as it flows from the entry cylinder towards the exit cylinder of the sensor, passing through the seven parallel tubes. Notably, the temperature of the water reaches 288 K within the tubes, indicating effective heating within the system. These results highlight the importance of understanding the temperature dynamics within the sensor, which can inform the optimization of the system for improved performance.

Figure 4 displays the distribution of water temperature along the two inlet cylinders and the outlet. The data shows that the temperature of the water circulating inside the inlet cylinder increases by 4 K between the first and seventh tubes, whereas the temperature at the outlet cylinder remains almost constant. This behavior is expected, as the water at the start of the cycle is relatively cold and gradually heats up until reaching thermal equilibrium towards the end of the cycle. Low flow rates are favorable in achieving thermal equilibrium as compared to higher flow rates. Therefore, understanding the temperature distribution and the effects of flow rates can aid in optimizing the system's design and operation to enhance thermal efficiency and improve overall performance.

Figure 5 depicts the evolution of water temperature profiles at the center of the sensor on the (X, Z) plane at 10:00 a. m., with ambient temperature T_{amb} = 278.95 K, direct normal irradiation D_i = 922 W/m², and diffuse horizontal irradiation D_H = 49 W/m².

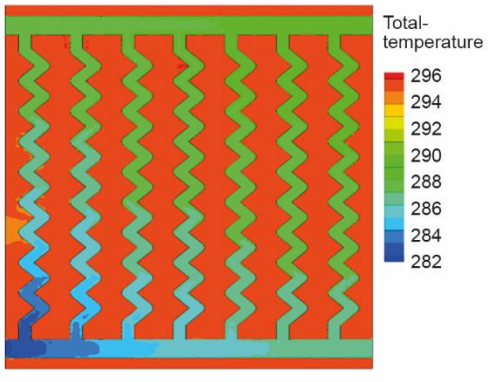

Figure 3. Temperature field 08:00 a. m., (T_{amb} = 274.75 K, D_i = 189 W/m², D_H = 7 W/m²)

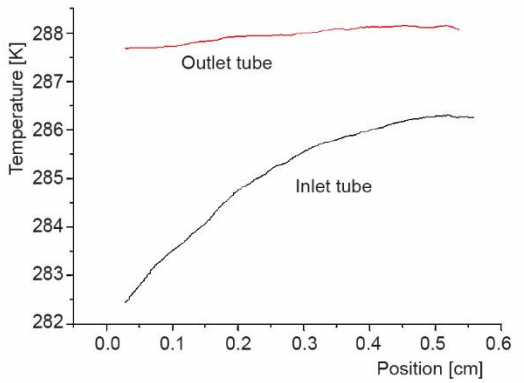

Figure 4. Evolution of the water temperature inside the inlet and outlet tubes at 08:00 a. m.

The results highlights the rapid increase in water temperature at the inlet cylinder, which is further increased as it passes through the seven Z-shaped tubes. This behavior results in the water reaching a temperature of 328 K at the outlet of the sensor, indicating effective heating of the fluid. These findings emphasize the importance of understanding the temperature dynamics within the sensor, as it can provide valuable insights into optimizing the system's design and operation for enhanced thermal efficiency and improved performance.

Figure 6 displays the temperature profile of water circulating within the inlet cylinder between the first and seventh Z-shaped tubes, indicating an increase of 12 K in temperature. In contrast, the temperature rise at the outlet cylinder is found to be only 1 K. These results suggest that while the heating efficiency is significant within the sensor, it is not fully optimized as thermal equilibrium is not achieved at the output due to higher energy input. Therefore, to enhance the thermal performance, it is recommended to regulate the water flow rate at the inlet to achieve optimal thermal equilibrium at the outlet. These observations are crucial for designing and operating the sensor with improved efficiency and performance.

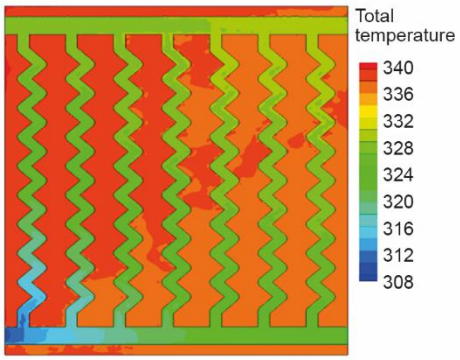

Figure 5. Temperature field 10:00 a. m. (T_{amb} = 278.95 K, D_i = 922 W/m², D_H = 49 W/m²)

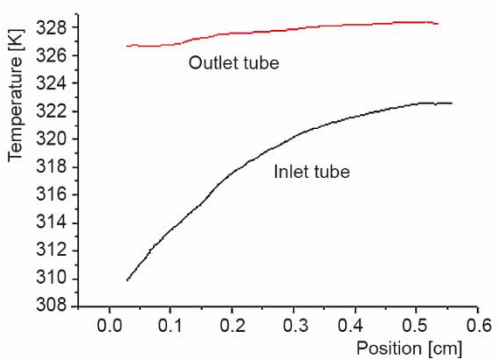

Figure 6. Evolution of the water temperature inside the inlet and outlet tube at 10:00 a. m.

At noon, fig. 7 illustrates the progression of water temperature profiles at the center of the sensor on the plane (X, Z), given an ambient temperature of T_{amb} = 285.95 K, direct normal irradiation of D_i = 1025 W/m², and diffuse horizontal irradiation of D_H = 60 W/m². The temperature of the water rapidly rises at the inlet cylinder and continues to increase as it flows through the seven Z-shaped tubes. At the outlet of the sensor, the water temperature peaks at 334.5 K.

As shown in fig. 8, the temperature of the water circulating inside the inlet cylinder has increased by a significant 12 K between the first and seventh tubes (Z-shaped), while at the outlet cylinder, the increase is only 2 K. However, achieving 100% thermal equilibrium at the output is still not possible due to the increasingly high energy received by the sensor, which leads to a higher temperature gradient. To optimize the performance of the sensor, it is recommended to adjust the water flow rate at the inlet to achieve a balance between energy absorption and heat dissipation, thus allowing the sensor to operate closer to the thermal equilibrium state.

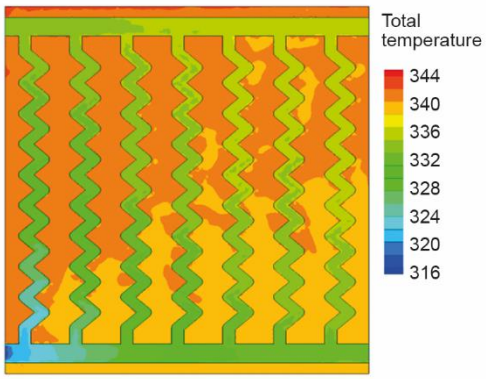

Figure 7. Temperature field 12:00 p. m., (T_{amb} = 285.95, D_i = 1025 W/m², and D_H = 60 W/m²)

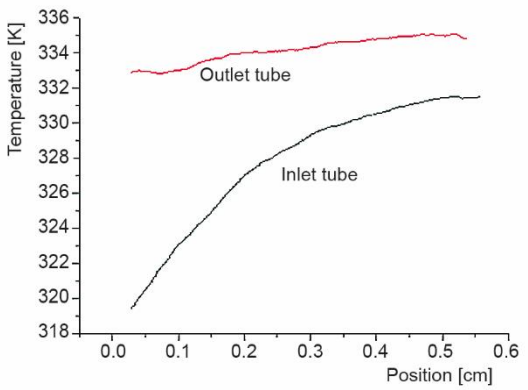

Figure 8. Evolution of the water temperature inside the inlet and outlet tube at 12:00 p. m.

The water temperature profiles at the center of the sensor on the (*X*, *Z*) plane at 02:00 p. m. are presented in fig. 9. The experimental conditions consisted of an ambient temperature of 291.15 K, direct normal irradiation of 1037 W/m², and diffuse horizontal irradiation of 60 W/m². It is observed that the temperature of the water increases sharply at the inlet cylinder and progressively rises as it passes through the seven Z-shaped tubes. Ultimately, the temperature reaches 356 K at the outlet of the sensor, indicating effective heat transfer within the system.

According to fig. 10, there is a significant increase in the temperature of the water as it circulates inside the inlet cylinder between the first tube (Z-shape) and the seventh tube (Z-shape), with an increase of 14 K. However, at the level of the output cylinder, the increase is only 2 K. This indicates that the thermal equilibrium is not fully achieved at the output due to the high energy received by the sensor. To optimize the thermal equilibrium and improve the efficiency of the system, it is recommended to reduce the water flow rate at the sensor inlet. The results obtained from this study provide valuable insights into the behavior of the sensor under different conditions, which can be useful in designing and optimizing similar systems.

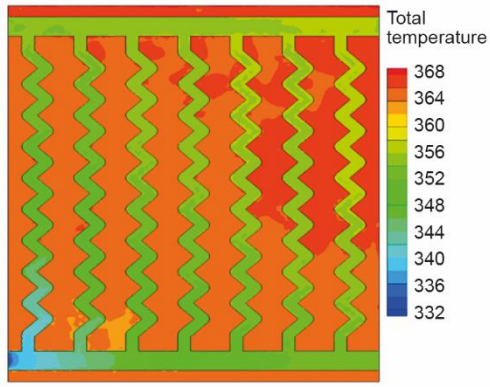

Figure 9. Temperature field 02:00 p. m., (T_{amb} = 291, D_i =1037 W/m², and D_H = 60 W/m²

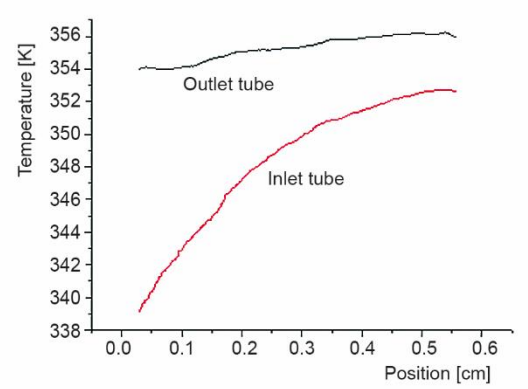

Figure 10. Evolution of the water temperature inside the outlet tube at 02:00 p. m.

At 4:15 p. m., fig. 11 exhibits the progression of the water temperature profiles at the center of the sensor on the (*X*, *Z*) plane. The ambient temperature is T_{amb} = 293.05 K, the direct normal irradiation is D_i = 901 W/m², and the diffuse horizontal irradiation is D_H = 55 W/m². It is observed that the water temperature rises rapidly at the inlet cylinder and is further augmented as it passes through the seven Z-shaped tubes, ultimately reaching 322 K at the outlet of the sensor.

According to fig. 12, the water temperature circulating within the inlet cylinder, specifically between the first and seventh tubes in the 'Z' formation, is expected to increase by a notable 0.8 °C. Conversely, at the output cylinder level, the temperature is projected to increase by a slightly higher 1 °C. These changes in temperature have important implications for the overall efficiency of the system, and should be closely monitored to ensure optimal performance.

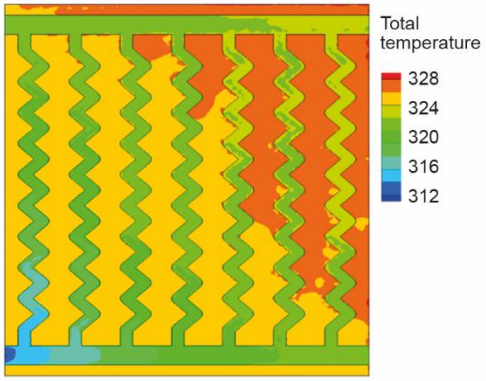

Figure 11. Temperature field 04:15 p. m., (T_{amb} = 293.15 K, D_i = 901 W/m², D_H = 55 W/m²)

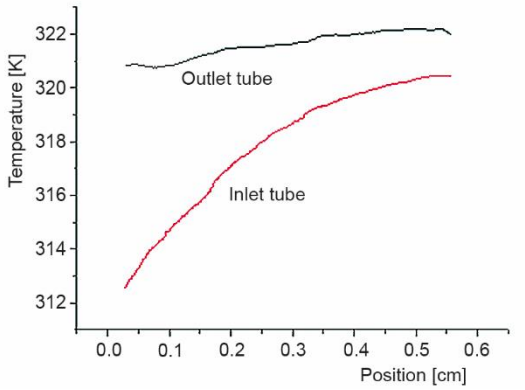

Figure 12. Evolution of the water temperature inside the outlet tube at 04:15 p. m.

At 6:00 p. m., fig. 13 presents a clear illustration of the water temperature profiles at the center of the sensor on the (*X*, *Z*) plane, taking into account various external factors. Specifically, with an ambient temperature of 292.25 K, direct normal irradiation of 406 W/m², and diffuse horizontal irradiation of 15 W/m², the data indicates a gradual increase in water temperature at the inlet cylinder, with the temperature eventually reaching 304 K.

In fig. 14, it is evident that there has been a significant increase in the temperature of the water circulating between the first and seventh tubes of the inlet cylinder, rising by a notable 3.5 °C. Meanwhile, the temperature of the outlet cylinder has increased by a more modest 0.5 °C. However, it is worth noting that this represents a slight decrease in temperature compared to measurements taken at 4:15 p. m. This decrease can be attributed to a drop in both direct normal irradiation, which has fallen to 495 W/m², and diffuse horizontal irradiation, which now stands at 40 W/m². The impact of these external factors on the system's performance underscores the importance of continuous monitoring and adjustments to optimize efficiency and maintain optimal performance.

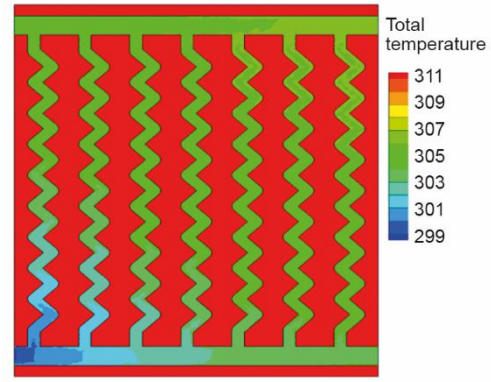

Figure 13. Temperature field 06:00 p. m., (T_{amb} = 292.25 K, D_i = 406 W/m², D_H = 15 W/m²)

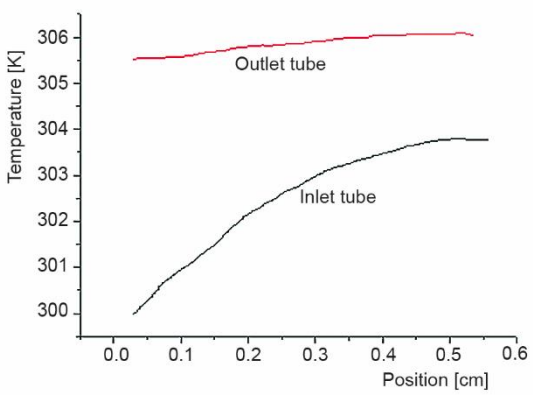

Figure 14. Evolution of the water temperature inside the outlet tube at 06:00 p. m.

At 8:00 p. m., fig. 15 provides a detailed visual representation of the water temperature profiles at the center of the sensor on the (X, Z) plane, taking into account ambient temperature, direct normal irradiation, and diffuse horizontal irradiation. In this case, the ambient temperature is 286.75 K, and the direct normal irradiation and diffuse horizontal irradiation are both recorded at 0 W/m². Despite these conditions, the temperature of the water in the inlet cylinder shows a gradual increase, reaching a temperature of 294.75 K. This indicates that the system is still functioning effectively, even in the absence of external energy sources, highlighting the importance of effective thermal management for sustained performance. Continuous monitoring of these factors will be crucial to ensure that the system operates at its optimal capacity.

According to fig. 16, the temperature of the water circulating between the first and seventh tubes of the inlet cylinder has increased by 3.5 °C, while the outlet cylinder has experienced a increase of 0.5 °C. However, due to the time of day, the sensor's overall performance is significantly diminished as it is currently night. The complete absence of both direct normal irradiation and diffuse horizontal irradiation, recorded at 0 W/m², underscores the im-

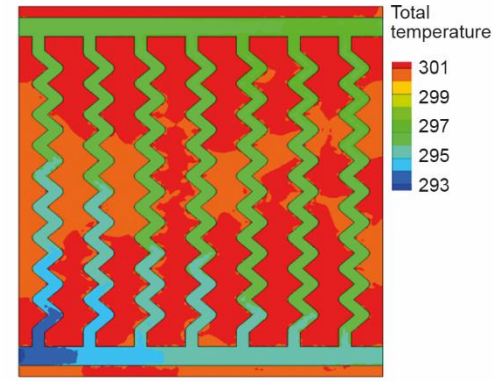

Figure 15. Temperature field 08:00 p. m., (T_{amb} = 286.75K, D_i = 0 W/m², D_H = 0 W/m²)

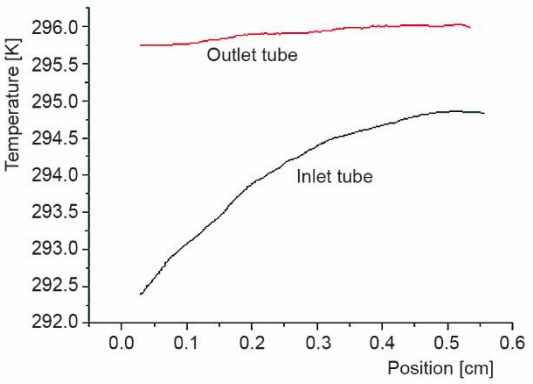

Figure 16. Evolution of the water temperature inside the outlet tube at 08:00 p. m.

portance of external energy sources in maintaining optimal performance. Despite these challenging conditions, the system is still able to achieve some degree of thermal management, highlighting the potential for continued improvements in efficiency and performance even in less-than-optimal conditions. Ongoing monitoring and refinement of the system design and operation will be key to unlocking its full potential.

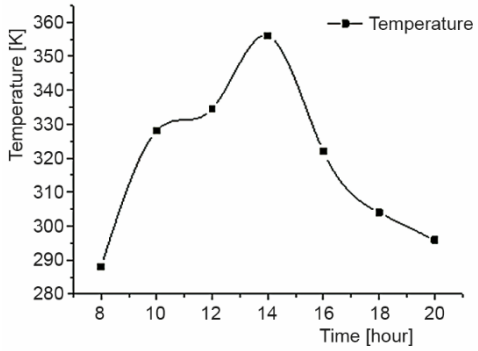

Figure 17. Evolution of water temperature during the day

Figure 17 provides a comprehensive view of the daily efficiency of the Z-tube solar water preheater, taking into account ambient temperatures ranging from 274.75-293.45 K. The graph reveals a clear pattern of increasing inlet and outlet temperatures of the collector from around 9:00 a. m. until reaching the maximum value of 356 K at 2:00 p. m. This upward trend corresponds to the period when solar radiation intensity is at its peak, driving optimal performance. However, as the intensity of solar radiation begins to decline, along with ambient temperatures, the inlet and outlet temperatures gradually start to decrease. This trend continues until the end of the collector cycle at 7:00 p. m.

Conclusions

This study aimed to investigate the thermal behavior of water flows in a solar collector equipped with zig-zag tubes using CFD. The simulation was performed using the finite volume method and the SIMPLE algorithm to discretize and solve the fluid domain. The simulation results demonstrated that the tube's shape significantly affects the flow behavior, which directly impacts the system performance. The inlet and outlet temperatures of the solar collector followed a clear pattern, increasing from 9:00 a. m. until reaching a peak of 356 K at 2:00 p. m., which corresponds to the peak solar radiation intensity. However, as the solar radiation intensity and ambient temperatures decrease, the inlet and outlet temperatures gradually start to decrease, and this trend continues until the solar collector cycle ends at 7:00 p. m. These findings underscore the importance of carefully managing external factors, such as solar radiation intensity and ambient temperatures, to maximize the system's efficiency. By continuously monitoring and adjusting these variables, the system's full potential as a sustainable and efficient source of thermal energy can be realized. In summary, the simulation results provide a comprehensive view of the daily efficiency of the Z-shaped tube solar water preheater, highlighting the significance of considering external factors to achieve optimal performance.

Acknowledgment

The authors Jihad Asad, Rabab Jarrar, and Hussein Shanak would like to thank Palestine Technical University-Kadoorie for supporting this work financially.

References

[1] Li, J., *et al.*, Technical And Economic Performance Study on Winter Heating System of Air Source Heat Pump Assisted Solar Evacuated Tube Water Heater, *Applied Thermal Engineering*, *221* (2023), Feb., 119851

[2] Tamuli, B. R., Nath, S. Analysis of Micro Heat Pipe Array Based Evacuated Tube Solar Water Heater Integrated with an Energy Storage System for Improved Thermal Performance. *Thermal Science and Engineering Progress*, *41* (2023), June, 101801
[3] Nazari, M., *et al.*, Exergy and Thermoeconomic Analyses of Serpentine Tube Flat-Plate Solar Water Heaters Coated With CuO Nanostructures, *Case Studies in Thermal Engineering*, *35* (2022), July, 102072
[4] Siritan, *et al.*, Thermal Performance and Thermo-Economics Analysis of Evacuated Glass Tube Solar Water Heater With Closed-Loop Pulsating Heat Pipe, *Case Studies In Thermal Engineering*, *35* (2022), July, 102139
[5] Tamuli, B. R., *et al*., Performance Enhancement of a Dual Heat Pipe Array Based Evacuated Tube Solar Water Heater for North Eastern India Climatic Condition: A Numerical Approach, *Applied Thermal Engineering*, *213* (2022), Aug., 118597
[6] Sivasubramanian, R., *et al.*, Performance Analysis of Multipass Tubes Solar Water Heater Using Nanofluids, *Materials Today: Proceedings*, *66* (2022), 3, pp. 1051-1055
[7] Gudeta, M. S., *et al.*, Performance Analysis of Solar Water Heater System With Heat Pipe Evacuated Tube Collector on Moha Soft Drink Industries in Ethiopia, *Case Studies in Thermal Engineering*, *36* (2022), Aug., 102211
[8] Arun, M., *et al.*, Experimental and CFD Analysis of Plain And Dimples Tube at Application of Solar Water Heater, *Materials Today: Proceedings*, *42* (2021), 2, pp. 804-809
[9] Al-Joboory, H. N. S. Comparative Experimental Investigation of Two Evacuated Tube Solar Water Heaters of Different Configurations for Domestic Application of Baghdad-Iraq, *Energy and Buildings*, *203* (2019), Nov., 109437
[10] Shalaby, S. M., *et al.*, Experimental Study of The Solar Water Heater Integrated With Shell and Finned Tube Latent Heat Storage System, *Journal of Energy Storage*, *31* (2020), Oct., 101628
[11] Deeyoko, L. A. J., *et al*., Exergy, Economics and Pumping Power Analyses of Flat Plate Solar Water Heater Using Thermal Performance Enhancer in Absorber Tube, *Applied Thermal Engineering*, *154* (2019), May, pp. 726-737
[12] Balaji, K., *et al.*, Experimental Analysis on Free Convection Effect Using Two Different Thermal Performance Enhancers in Absorber Tube of a Forced Circulation Flat Plate Solar Water Heater, *Solar Energy*, *185* (2019), June, pp. 445-454
[13] Tang, R., Yang, Y., Nocturnal Reverse Flow in Water-In-Glass Evacuated Tube Solar Water Heaters, *Energy Conversion and Management*, *80* (2014), Apr., pp. 173-177
[14] Wannagosit, C., *et al.*, Validated Mathematical Models of a Solar Water Heater System with Thermosyphon Evacuated Tube Collectors, *Case studies In Thermal Engineering*, *12* (2018), Sept., pp. 528-536
[15] Li, K., *et al.*, Numerical Investigation of Flow And Heat Transfer Performance of Solar Water Heater With Elliptical Collector Tube, *Energy Procedia*, *70* (2015), Apr., pp. 285-292
[16] Arab, M., Abbas, A., Model-based Design and Analysis of Heat Pipe Working Fluid for Optimal Performance in A Concentric Evacuated Tube Solar Water Heater, *Solar Energy*, *94* (2013), Aug., pp. 162-176
[17] Menni, Y., *et al.*, Effect of Wall-Mounted V-Baffle Position in A Turbulent Flow Through a Channel: Analysis of Best Configuration for Optimal Heat Transfer, *International Journal of Numerical Methods for Heat & Fluid-flow*, *29* (2018), 10, pp. 3908-3937
[18] Menni, Y., *et al.*, Enhancement of the Turbulent Convective Heat Transfer in Channels Through The Baffling Technique and Oil/Multiwalled Carbon Nanotube Nanofluids, *Numerical Heat Transfer, Part A: Applications*, *79* (2020) 4, pp. 311-351
[19] Vural, E., *et al.*, Analyzing the effects of hexane and water blended diesel fuels on emissions and performance in a ceramic-coated diesel engine by Taguchi optimization method, *Fuel*, *344* (2023), July, 128105
[20] Patel, A., *et al.*, Comparative Thermal Performance Studies of Serpentine Tube Solar Water Heater With Straight Tube Solar Water Heater, *IOSR Journal of Mechanical and Civil Engineering (IOSR-JMCE)*, *13* (2016), 4, pp. 79-83

Paper submitted: November 29, 2022
Paper revised: April 1, 2023
Paper accepted: April 26, 2023